Journal of the Korean Ceramic Society (2023) 60:747–759
https://doi.org/10.1007/s43207-023-00305-5

REVIEW

Review of the thermally stimulated depolarization current (TSDC) technique for characterizing dielectric materials

Hyunseok Song[1] · J. Pundareekam Goud[1] · Jiwon Ye[1] · Wonsik Jung[2] · Jaehoon Ji[2] · Jungho Ryu[1,3]

Received: 15 February 2023 / Revised: 30 March 2023 / Accepted: 5 April 2023 / Published online: 18 April 2023

Abstract
Atomic defects, particularly oxygen vacancies, affect the charge transport mechanisms and DC resistance changes in dielectric materials; therefore, their concentrations and distributions are crucial for understanding the electrical property deterioration of materials. The thermally stimulated depolarization current (TSDC) technique has been introduced to investigate the behavior and characteristics of atomic defects in dielectric materials, which is one of the best and most widely used methods among various techniques. The relaxation type including dipoles, trap charges, and mobile ions, and the concentration of defects in dielectrics can be determined through information such as maximum temperature (T_m), and maximum current density (J_m) from each peak in the TSDC results and activation energy (E_a) calculated from the slope. In this review, an overview of the TSDC technique, including fundamental theory, characterizing procedures such as poling processes and current measurement during depolarization, an analytical method according to the variables, and applications to various dielectric systems, is presented.

Keywords Thermally stimulated depolarization current · Defect relaxation · Dielectric · Activation energy · Dopant

1 Introduction

Dielectric materials have attracted considerable attention to meet the increasing demand for various applications such as capacitors, semiconductor devices, voltage-controlled oscillators, resonators, and transducers owing to their high electrical energy storage capacity, excellent power conditioning, high permittivity, high tunability, and electrical functionality [1–6]. A high dielectric constant, high dielectric breakdown strength, and high reliability are required for various applications using dielectric materials [7–10]. Defect behavior, which is strongly related to dielectric polarization and relaxation, plays a critical role in estimating the dielectric properties [11–13]. For example, the mobility of impurity ions induces space-charge polarization in dielectrics, resulting in easy dielectric relaxation accompanied by electrical degradation. Thus, an investigation of the dielectric relaxation caused by atomic defect behavior in a dielectric material is necessary to determine the performance of dielectric materials and their suitability and reliability for specific applications [14–16].

To understand dielectric relaxation, various analytical techniques have recently been reported, such as atomic-scale simulations/theoretical calculations based on defect chemistry and electrostatics, chemical analysis such as energy dispersive spectroscopy and electron energy loss spectroscopy (EELS), electrical measurements such as complex impedance spectroscopy, current–voltage (I–V) behavior, and highly accelerated lifetime tests (HALT), among other sophisticated microscopic analysis techniques [17–22]. However, these methods cannot exclude the influence of external factors, such as electric fields, on the polarization state based on the defects, resulting in poor sensitivity; in addition, the dipoles and charges are still immobile at low temperatures [23]. Therefore, it is difficult to achieve high reliability when analyzing the defect behavior of dielectrics.

Hyunseok Song and J. Pundareekam Goud have contributed equally to this work.

✉ Jungho Ryu
jhryu@ynu.ac.kr

[1] School of Materials Science and Engineering, Yeungnam University, Gyeongsan 38541, Korea

[2] Corporate R&D Institute, Samsung Electro-Mechanics, Suwon 16674, Korea

[3] Institute of Materials Technology, Yeungnam University, Gyeongsan 38541, Korea

The thermally stimulated depolarization current (TSDC) technique is an important complementary tool to identify dielectric relaxation processes as a function of temperature, charge storage or decay processes, and in-grain/inter-grain defect mobility with high resolution [24]. The current generated through the heat-stimulated discharge during the TSDC measurement exhibited several specific peaks. By analyzing the shape and location of these peaks, including information on the slope, maximum temperature (T_m), and maximum current density (J_m) of the peaks, the characteristics of the relaxation type (dipoles, trap charges, and mobile ions), nature, and concentration of defects in dielectrics can be interpreted [24–29]. The TSDC can also evaluate the activation energy and time of relaxation to quantify the physical mechanisms of the defect behavior [30–32].

This review article presents an overview of the TSDC technique, including the method to estimate the mechanism, cause, and type of defect by analyzing the information on the maximum temperature (T_m) and maximum current density (J_m) in each peak of the TSDC results, and the concentration of defects in dielectrics determined by calculating the activation energy (E_a) from the peak shape. The practical TSDC measurement procedure, including polarization and depolarization for monitoring the leakage current from the dielectrics, is summarized. Because the analysis method of TSDC results can be extended to other various material systems, such as polymers, single crystals, and ceramics, beyond dielectrics, other applications of TSDC are provided in this review article.

2 Fundamental theory of TSDC

This section discusses the basic theory and equations used for TSDC measurements and experimental data interpretation. As mentioned, TSDC is a powerful technique used to investigate the effects of defect type and concentration on the electrical conduction and degradation of a dielectric material. The charge transport mechanisms in dielectric materials were explored in terms of the migration of oxygen vacancies under a DC bias. The TSDC result of the dielectric material typically shows three current density peaks (A, B, and C) as a function of temperature, as shown in Fig. 1a. By analyzing information such as the peak temperature (T_m) and peak current density (J_m) of each peak, the causes and mechanisms of the dipole, trapped charge, and space charge, among others, can be calculated, and the concentration of the defects can be determined by calculating the activation energy (E_a) from the peak shape [27, 28, 33]. Peak A is affected by the relaxation of the permanent dipole at the phase transition temperature. Peak A is determined to be of relaxation by the defect dipole origin caused by trapped charge, except for the effect of oxygen vacancy ($V_O^{\cdot\cdot}$)-based relaxation, as described in Fig. 1b. Peak A is not affected by the electric

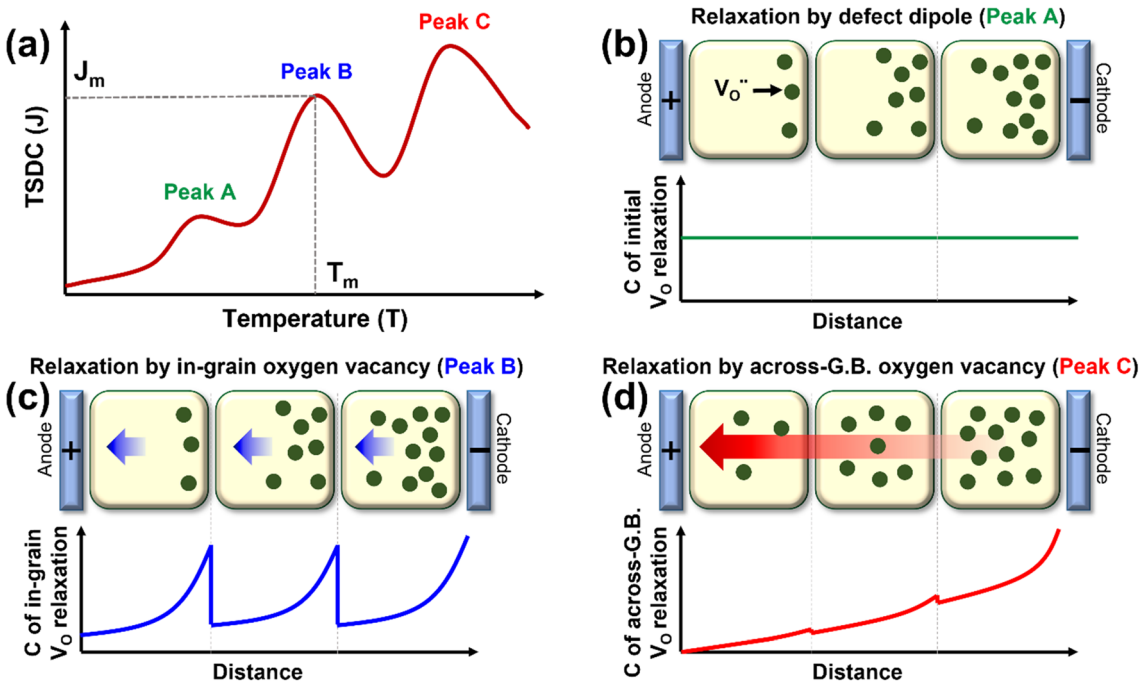

Fig. 1 **a** Conceptual schematic result of TSDC measurement showing the information of peak current density (J_m) and peak temperature (T_m) of each peak (Peak A, B, and C). Schematic behavior and concentration of oxygen vacancy during the relaxation (**b**) by defect dipole, **c** in-grain oxygen vacancy, and **d** across-grain boundary (G.B.) oxygen vacancy

field or poling temperature because it is based on the internal characteristics of the material itself, such as the composition of the dielectric material and the type and concentration of the dopant. Peaks B and C represent relaxation by oxygen vacancies related to space charge, which is affected by poling conditions, including the temperature and electric field. Therefore, the information from Peak B can be used as basic data to investigate the relaxation of in-grain oxygen vacancies, as shown in Fig. 1c. When the concentration and mobility of oxygen vacancies in the grain are high, J_m is high and T_m is low in Peak B, and E_a which is calculated from the shape of Peak B is low. Peak C can provide information on oxygen vacancy relaxation across the grain boundaries (G.B.), as presented in Fig. 1d. When the concentration and mobility of oxygen vacancies serving as charge carriers in dielectrics are high, high J_m and low T_m are shown in Peak C, and the low value of E_a is determined from the shape of Peak C. The concentration distribution of oxygen vacancies through the grains during relaxation is schematically described in Fig. 1b–d [23, 28, 32–36].

J_m provides information on the concentration and mobility of defect dipoles and oxygen vacancies that act as charge carriers during relaxation with increasing temperature. A high J_m indicates a high concentration or high mobility of defects such as oxygen vacancies, which carry charges during relaxation [5, 24, 32, 37]. The current density during relaxation can be theoretically presented as the following equation [24, 38–41]:

$$J(T) = Cn_0 s \exp\left(-\frac{E_a}{kT}\right) \times \exp\left[{}^{s}/_{\beta} \int_{T0}^{T} \left(-\frac{E_a}{kT}\right) dT\right], \quad (1)$$

where J is the current density, C is the geometry constant, n_0 is the concentration of dipoles, s is the frequency factor, E_a is the activation energy of the process, k is Boltzmann's constant, β is the heating rate, T is the absolute temperature, and T_0 is the initial temperature. This approach is based on the observation that for $T \leq T_m$, the integral term in Eq. (1) is negligibly small. Therefore, only the processes that occur at lower temperatures are important, and the first exponential factor in Eq. (1) is most important in the low-temperature part of the TSDC curve where it starts. Equation (1) allows the calculation of the dipole concentration n_0. In this case, the Arrhenius equation can express the current density during the thermally stimulated measurement. Using this technique, it is also possible to determine the activation energy (E_a), defect concentration, and relaxation time. The origin of each peak and the information obtained from each peak are summarized in Table 1.

T_m is the temperature at which dielectric relaxation occurs maximally to obtain the maximum current density [42]. A high T_m means that high thermal energy is required to induce relaxation, and thus, the mobility of defects is low in dielectrics. T_m is defined as [33, 43]:

$$T_m = \sqrt{\frac{qE_a}{kv(T_m)}}, \quad (2)$$

where v is the relaxation frequency, q is the heating rate, k is Boltzmann's constant, and E_a is the activation energy of the process.

The current density and maximum temperature were directly related to the activation energy (E_a). E_a is the minimum energy required to generate depolarization by the defect dipole and oxygen vacancy. When the concentration and mobility of the defects are low, the E_a appears to be of low intensity. E_a of the TSDC peak was determined through three distinct methods: the initial rise model, full width at half maximum (FWHM) method, and different heating rates [42]. First, using the TSDC polarization field dependence and the initial rise method (Fig. 2a) [24, 41, 44], each TSDC peak was assigned to a different polarization mechanism. The Bucci–Fieschi theory [45] can be used to explain the relaxation process during TSDC measurements, and the initial rise [46] approach can be used to determine

Table 1 Origin of each peak and information can be obtained from each peak in the TSDC result

	Peak A (defect dipole)	Peak B (in-grain oxygen vacancy)	Peak C (across-G.B. oxygen vacancy)
Peak position; maximum temp (T_m)			
Information	Type of defects		
Origin	Temp. to induce enough driving force (> E_a) for defect migration (Peak A is related to phase transition near the Curie temperature)		
Peak magnitude; current density (J_m)			
Information	Concentration and mobility of defects		
Origin	Leakage current by migration of defect during depolarization		
Peak shape; activation energy (E_a)			
Information	Relaxation kinetics of defects (type, concentration, and mobility of defects in specific material)		
Origin	Minimum energy to induce the migration of defects		

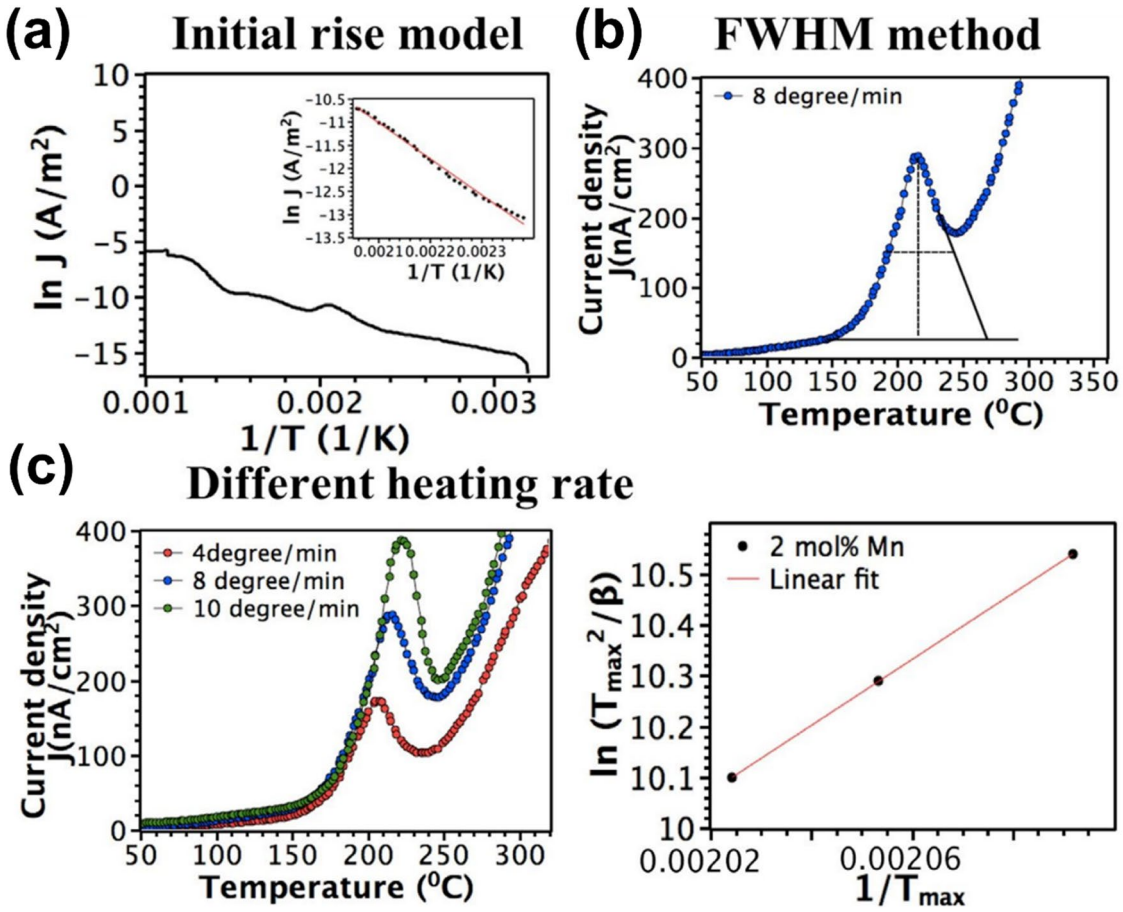

Fig. 2 Calculating the activation energy from the TSDC result: **a** Initial rise model, **b** FWHM method, and **c** different heating rate [42]. Copyright 2021, Journal of the American Ceramic Society

the polarization E_a for the defects in the following equation [32, 37, 47, 48]:

$$-\ln\left[\frac{J(T)}{Const.}\right] = \frac{E_a}{KT} + \exp\left[\frac{E_a}{kT_m} - \frac{E_a}{kT}\right], \tag{3}$$

$$-\ln[J(T)] \cong \text{Const.} - \frac{E_a}{KT}. \tag{4}$$

E_a can be determined from the slope of the plot *J(T)* vs. *1/T*. In the second technique, the FWHM of the TSDC peak was used to calculate E_a (Fig. 2b) using the following equation [49]:

$$E_a = \frac{2.30k_bT_m^2}{\Delta T_{\frac{1}{2}}}, \tag{5}$$

where k_b is Boltzmann's constant, T_m is the maximum temperature at the TSDC peak, and $\Delta T_{1/2}$ is the FWHM of the TSDC peak. Third, a different heating rate method is utilized depending on the heating rate of the TSDC peak to resolve the E_a of the TSDC relaxation current (Fig. 2c), which is calculated using the Arrhenius equation described by the following equations [50]:

$$\ln\beta = \frac{-E_a}{k_b}\left(\frac{1}{T_m}\right) + const, \tag{6}$$

$$\text{Ln}\left(\frac{T_m^2}{\beta}\right) = \frac{E_a}{k_bT_m} + \ln\left(\frac{\tau_0E_a}{k_b}\right), \tag{7}$$

where β is the heating rate, k_b is Boltzmann's constant, T_m is the maximum temperature at the TSDC peak, and τ_0 is the characteristic relaxation time. E_a can be used to investigate the relaxation kinetics of tapped charges, defect dipoles, or ionic space. The estimated activation energies from all three methods were in good agreement with those for the migration of oxygen vacancies [42].

The TSDC spectra can be used to calculate the characteristic relaxation time (τ_0), which is another important

parameter. This equation can be used to characterize the relaxation time of the polarized species [40, 51].

$$\tau(\mathrm{T}) = \tau_0 \exp\left(\frac{E_a}{KT}\right), \tag{8}$$

where the reciprocal of the frequency components is the relaxation time (τ) at infinite temperature, and if $dJ(T)/dT = 0$ at $T = T_m$, the relaxation time (τ_0) can be transformed into the following equation [27, 28]:

$$\tau_0 = \frac{1}{S} = \frac{kT_m^2}{E.a} \exp\left(-\frac{E}{KT}\right), \tag{9}$$

where τ_0 is the characteristic relaxation time and τ is the relaxation time of the polarized species. Generally, the heating rate impacts the position and shape of the TSDC peaks. As the heating rate increased, the TSDC peak narrowed and shifted to higher temperatures. Higher depolarization currents result from enhanced dipolar interactions after relaxation at high heating rates [28, 51].

3 Experimental procedure of TSDC measurement

The TSDC method is based on the depolarization of a material caused by heat activation. Figure 3a depicts the general testing setup for the TSDC measurements, which includes a high-voltage supply for poling the dielectric sample under a high electric field, a current meter for evaluating the leakage current from the dielectrics during depolarization, and an environmental chamber for polarization and *in-situ* leakage current measurement with temperature control. To characterize the current induced by depolarization by thermal stimulation, the specimen should be dielectrically poled before heating. First, a sample is heated to the poling temperature (T_P) and kept there for a certain period of time (t_P) long enough to allow the various mobile entities in the material to position themselves (electrical poling) under an electric field (E_P), as described in Fig. 3b [24, 51]. Two different types of polarization can occur at this stage. One is dipolar polarization, which is the orientation of dipoles in the direction of the applied field, and the second is space-charge polarization, which is the mass movement of charges (electrons, holes, and ions) through the majority of the sample [52]. The possible defects in the material respond to this field stress by forming a metastable state of charge or dipole distribution. Subsequently, the sample was rapidly cooled to a lower temperature (T_0) to freeze polarized defects. To eliminate any potential surface charges and stabilize the sample at this temperature, it should be short-circuited for a particular time, and the polarizing electric field should be withdrawn to depolarize some polarizations with a short relaxation time. Owing to the increased mobility, free electrons, and holes can swiftly conduct across the metal electrode. Polarized ionic defects have a lower movement velocity owing to the blockage of metal electrodes by ionic species such as oxygen vacancies ($V_O^{\cdot\cdot}$) [42, 51]. As the temperature increased, these charge distributions or polarized states relaxed. This is because the thermal energy excites the lattice vibrations, which initiate the charged motion or align dipoles. This results in a small current flow to the external measurement circuit, measured as the TSDC [51, 53].

The parameters of the poling process, such as the polarization temperature and polarization field, can affect the result obtained by the TSDC, especially the peak shape. From the peak shape affected by the condition of poling, including the information of J_m and T_m, the type of defect can be determined, and E_a can be calculated. For example, the intensity of J_m shows a slight increase at Peak A and a large increase at Peak B with an increase in the polarization field in the same sample, as shown in Fig. 4a [29],

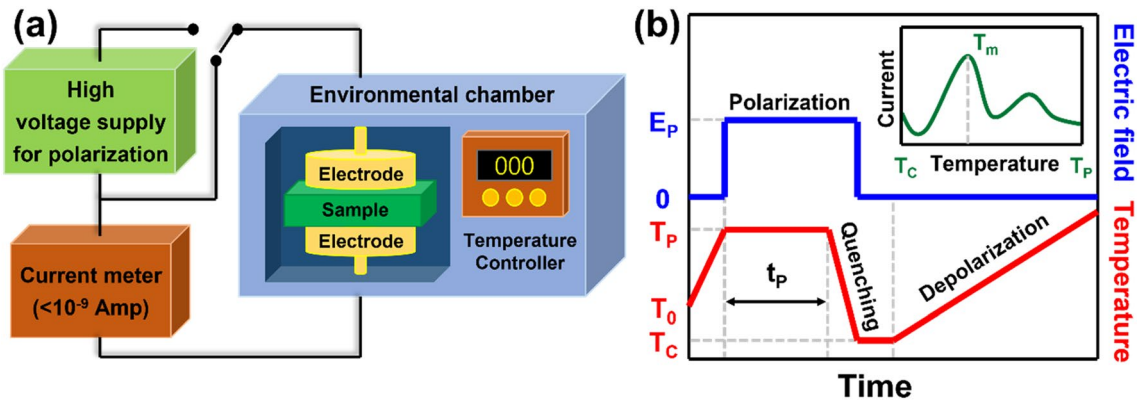

Fig. 3 **a** Schematic of TSDC measurement setup and **b** thermal and electrical process profiles of polarization and depolarization during TSDC measurement

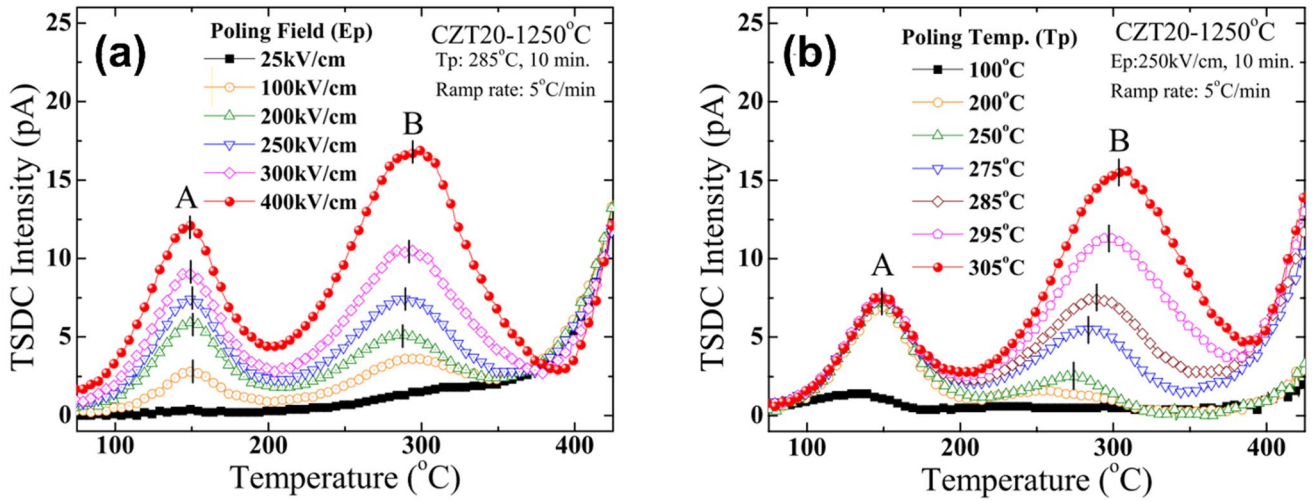

Fig. 4 TSDC results depending on (**a**) the poling field (E_p), and **b** the poling temperature (T_p) [29]. Copyright 2013, Journal of the American Ceramic Society

which means that the relaxation at Peak B is more dependent on the polarization than that at Peak A. Furthermore, the dependency on space-charge depolarization is larger than that of trap charge depolarization [37]. The T_m at Peak A decreases and T_m at Peak B increases with increasing polarization field, as shown in Fig. 4b [29] T_m decreases with an increase in the polarization field because the relaxation current is related to the trapping charge, whereas T_m increases with an increase in the polarization field when the relaxation is caused by the space charge. Based on this fact, Peak A is related to defect dipole relaxation, and Peak B is based on the relaxation of oxygen vacancies. The type of defect can be determined by evaluating the E_a level of each peak. For example, by comparing the theoretical dipole trap charge, E_a, or in-grain or across-grain boundary (G.B.) oxygen vacancy space charge E_a of a specific material system with the relaxation activation energy of each peak, the type of relaxation at each peak can be determined, as presented in Fig. 5 [5].

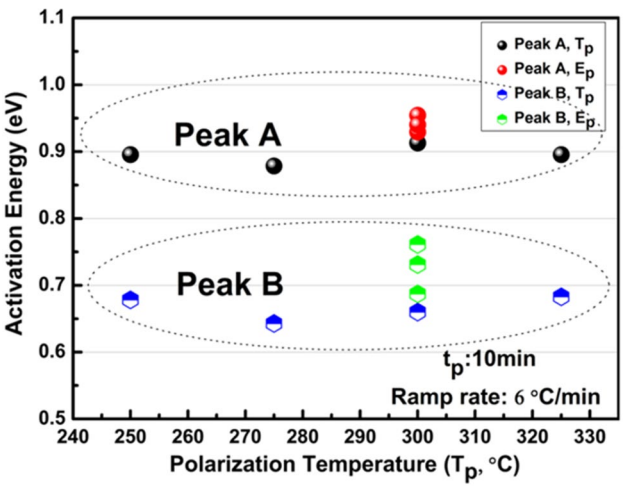

Fig. 5 Calculated results of activation energy during relaxation with a variation of polarization temperature (T_p) to distinguish Peak A (defect dipole relaxation) and Peak B (oxygen vacancy relaxations) [5]. Copyright 2014, Journal of the American Ceramic Society

4 Effect of parameters on the TSDC in dielectric materials

4.1 Influence of the poling condition on the TSDC

An example showing the influence of poling conditions on the TSDC results reported by Shi et. al is presented in Fig. 6. TSDC examined how to charge distribution and interfacial properties contribute to dielectric loss in polyethylene (HDPE) composites filled with $Mg_{0.95}Ca_{0.05}TiO_3$ (MCT) [54]. The measurement was carried out according to the TSDC spectra under various polarization settings. Charges are frequently trapped in trap sites (such as interfacial areas) when composite materials are subjected to an external field. The relative permittivity and dielectric loss of the composites were measured for their temperature dependency, and it was shown that the dielectric loss strongly depended on the temperature. The release of charges that have built up in the interfacial area during heating is thought to be a factor in the increased dielectric loss that occurs as the temperature increases. TSDC graphs of the sintered MCT ceramics with a fixed polarization field of 200 V/mm and various polarization temperatures are shown in Fig. 6a. T_P was set to 100, 200, 300, and 400 °C. The spectra consist of two distinct peaks, denoted

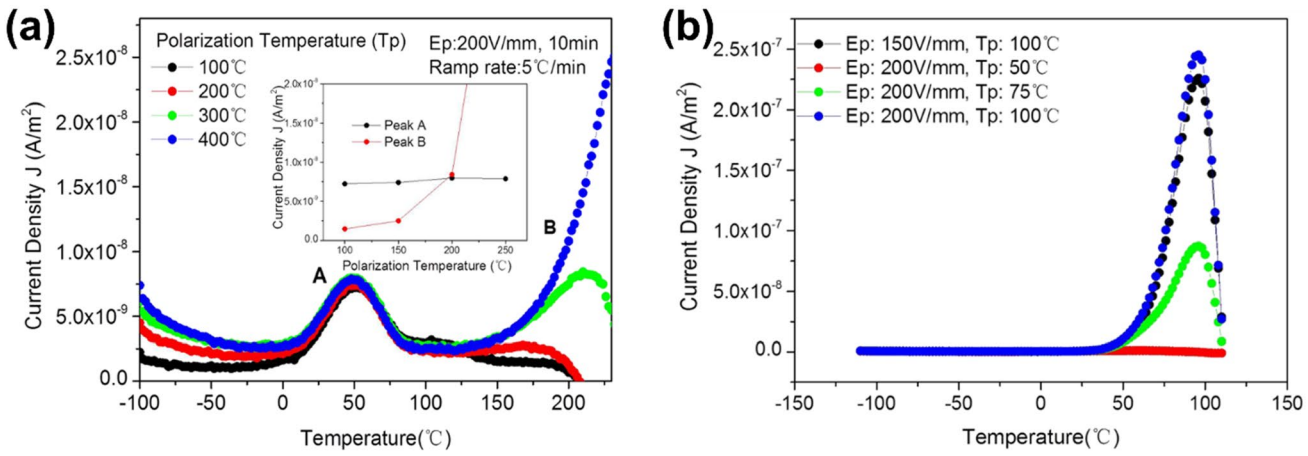

Fig. 6 TSDC plots for **a** sintered MCT ceramic depending on the polarization temperature (T_p) and **b** pure HDPE under different T_p and polarization fields (E_p) [54]. Copyright 2017, AIP Advances

A and B, indicating that the MCT has at least two different types of defects.

The specifics of Peaks A and B at each polarization temperature are plotted in Fig. 6a (inset) to clearly understand their origin, as the variation in position and intensity of the TSDC peak is the basis for categorizing defect types. Peak A is unaffected by the increase in polarization temperature in terms of either location or intensity, suggesting that it is related to the relaxation of defect dipoles, such as (Ti'_{Ti})-$(V_O^{\cdot\cdot})$ [29]. The peak A current density maintained a constant value of 8×10^{-9} A/m^2. In contrast, Peak B could not be produced until T_P was increased to 300 °C, and as T_P increased, the intensity of Peak B increased as well. Under harsher polarization conditions, the position of Peak B shifted to a higher temperature range, accompanied by a sharp increase in current density, which is a sign of polarization due to the movement of oxygen vacancies [27, 55]. In comparison, pure HDPE was subjected to TSDC measurements at a set $E_P = 200$ V/mm. The spectrum at $T_P = 50$ °C is essentially flat, as shown in Fig. 6b. A distinct peak could not be seen around 90 °C until the polarization temperature was increased to 75 °C. If T_P is raised to 100 °C, a higher peak within the same temperature range appears, and the peak value rises to 2.510^{-7} A/m^2. The TSDC peak attained under a lower polarization field of 150 V/mm is less significant than that of 200 V/mm at a given polarization temperature of 100 °C. These indications from the plots imply that the peak is the result of charges injected from the electrodes and that the current density may be related to the number of injected charges [56].

Studies of trap properties in oxide semiconductors and organic polymers demonstrated the field dependency characteristics of TSDC peak positions [28, 29]. With rising polarization, the T_m value of Peak A does not remain constant and shifts toward low temperatures, according to the T_p dependence and E_p dependence of the depolarization current. Therefore, the trap space charges are related to the observation of Peak A. The change in Peak A during the TSDC tests reflects the dielectric thermal release of trap charges. For Peak B, the increase in the relaxation peak temperature (T_m) is the same as that in J_m, which is caused by more intense polarization. This occurrence fits the definition of space-charge polarization as a whole. Therefore, the relaxation of mobile oxygen vacancies is thought to be the primary cause of Peak B [24, 32, 56, 57].

4.2 Analysis of peaks to decide the type of defect

The relationships between thermally stimulated relaxation and defect behavior can be characterized by TSDC spectra, such as that discussed for $BaTi_4O_9$ microwave dielectric ceramics [32]. Both the TSDC curves and dielectric spectra for $BaTi_4O_9$ showed relaxation caused by heat. The main defect types in the $BaTi_4O_9$ ceramics were defecting dipoles (Ti'_{Ti})–$(V_o^{\cdot\cdot})$ and oxygen vacancies $(V_o^{\cdot\cdot})$, specifically the in-grain and across-grain boundary oxygen vacancies, which were also responsible for the thermally simulated relaxation at low and high temperatures [32].

The TSDC curves for polarized $BaTi_4O_9$ ceramics at various T_P between 150 and 250 °C with a constant DC E_P of 100 V/mm are shown in Fig. 7 a and b. Each TSDC curve has three different peaks (A, B, and C), which shows that $BaTi_4O_9$ has at least three ways for the defects to relax. This behavior is similar to the TSDC relaxation of TiO_2 ceramics at low temperatures [32, 58]. Because the dipole current decreases with longer depolarization times, the dissociation of defect dipoles (Fe'_{Ti})–$(V_o^{\cdot\cdot})$ occurs. These results show that the defect dipoles (Peak A) become unstable when there

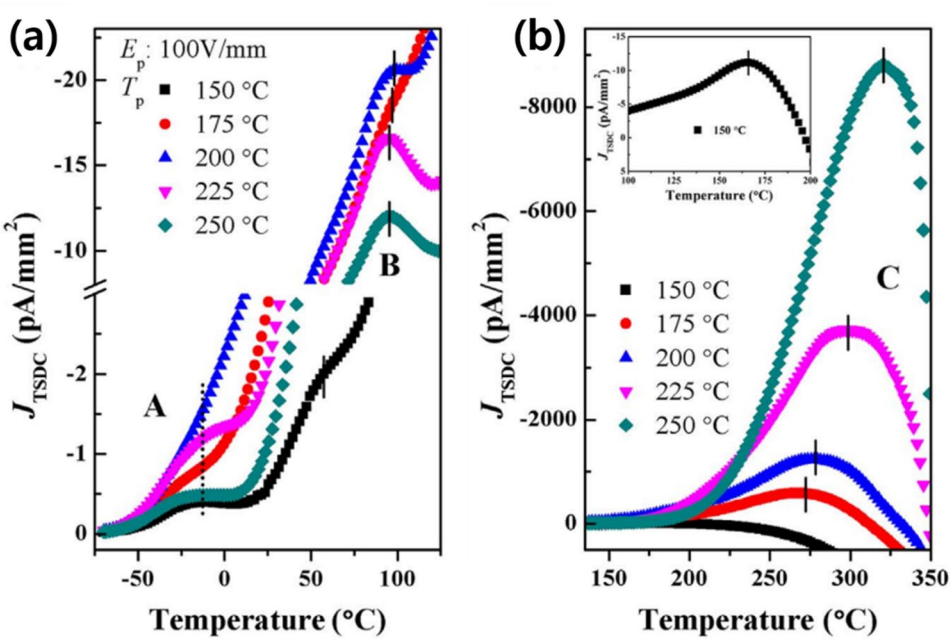

Fig. 7 TSDC spectra under different polarization temperatures (T_p) from 150 to 250 °C at a fixed polarization field (E_p) of 100 V/mm: **a** – 25–125 °C, and **b** 150–350 °C [32]. Copyright 2017, Materials & Design

is more polarization. The activation energy (E_a) calculated at Peak A is between 0.32 and 0.36 eV, which is near the energy value at which TiO_2 ceramics undergo low-temperature TSDC relaxation. This suggests that the equivalent relaxations of $BaTi_4O_9$ and TiO_2 ceramics may have similar physical origins [58]. As the sample was heated, oxygen vacancies were pushed by the temperature to move over the barriers of the grains and grain boundaries. This is called "in-grain migration" [27, 58] and "across-grain boundary migration." In-grain and across-grain boundary oxygen vacancies ($V_o^{\cdot\cdot}$) appeared at higher temperatures, with E_a of 0.30–0.48 eV at Peak B and 0.65–1.01 eV at Peak C, respectively. The dielectric relaxation observed at low and high temperatures was caused by two types of defects, (Ti'_{Ti})–($V_o^{\cdot\cdot}$) and ($V_o^{\cdot\cdot}$), respectively.

4.3 Analysis of activation energy to decide the dipole concentration

The TSDC technique was conducted on the Fe-doped $SrTiO_3$ model system to evaluate the concentration of dipoles in the dielectric system [17]. In the temperature window considered in this study, the three peaks have different bias-dependency characteristics, which shows that a different defect causes each peak. As shown in Fig. 8, these three peaks were determined to be the relaxation of polarized dipoles, traps, and oxygen vacancies, based on the peak position and magnitude properties under different polarization conditions [33]. The defect dipoles with a computed activation energy (E_a) of 0.76 ± 0.05 eV and an estimated dipole concentration of 10^{19} cm^{-3} are responsible for the low-temperature TSDC Peak A. The second Peak B is recognized as the space-charge peak, which has a trap center. Using the curve-fitting approach, the trap density for a 1% Fe-doped sample was determined to be 2×10^{14} cm^{-3} and E_a was 0.65 ± 0.08 eV.

The high-temperature Peak C is attributed to the relaxation of oxygen vacancies since it exhibits the typical parabolic bias dependency, thickness dependence, and E_a of 0.91 ± 0.05 eV. According to the collecting bias investigation, a small bias applied in the direction opposite to the internal field created by the oxygen vacancies and interfacial traps can prevent the relaxation of oxygen vacancies during the heating step. The concentrations of defect dipoles in crystals with concentrations of 0.1% and 1% Fe dopant were examined in this study. The concentration of dipoles, n_0, for a TSDC peak caused by dipole orientation can be calculated using Eq. (1). By integrating the area under Peak A, the estimated dipole concentration for a sample with 0.1% Fe doping is 1.6×10^{19} cm^{-3} and that for a sample with 1% Fe doping is 6.6×10^{19} cm^{-3}. The accompanying fluctuation in dopant concentration did not result in the expected factor of 10 differences in the dipole concentration. The different Fe valence states and intricate arrangements of defect dipoles in the lattice can impact this discrepancy.

Although it is challenging to distinguish the types of defects due to the similarity of the activation energies for each peak, the type of defects can be determined by analyzing the dependence of the peak position on the polarization condition. In Fig. 8, the position of Peak A remains at a constant T_m with different E_p, indicating that it is related to the defect dipole and is not significantly affected by the intrinsic elements of the material. On the other hand, the position of Peak B shifts to a lower temperature with

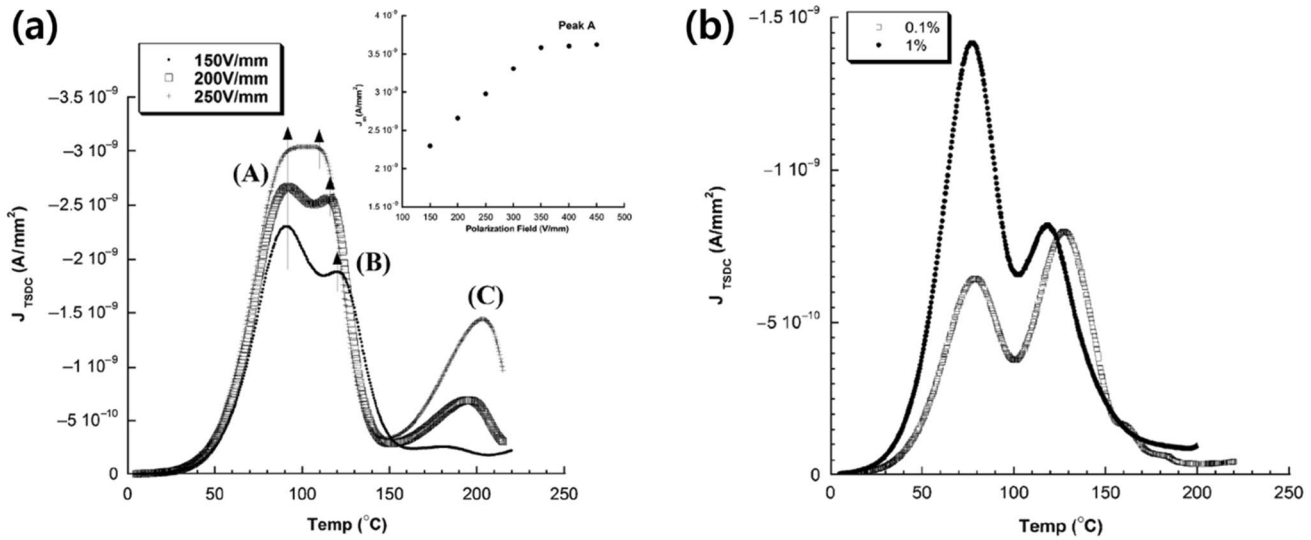

Fig. 8 **a** TSDC spectra on FE-doped $SrTiO_3$ crystal with polarization field (E_p) of 150–250 V/mm at a fixed polarization temperature (T_p) of 100 °C. Dashed arrows indicate the maximum peak current positions, T_m (Inset: polarization field dependence of J_m of Peak A). **b** TSDC spectrum of 0.1% and 1% Fe-doped $SrTiO_3$ single crystals, $E_p = 100$ V/mm [33]. Copyright 2008, Journal of the American Ceramic Society

increasing intensity of E_p, suggesting that the dielectric thermal release of trap charge during depolarization begins at an earlier stage when defect ions acquire higher energy under higher polarization electric fields.

5 Applications of TSDC

The TSDC approach is a potential tool for both qualitative and quantitative understanding of defect characteristics in dielectric materials, especially ceramics. For decades, it has been extensively used to describe the relaxation mechanisms of polymers [51, 54]. It is useful in polymer research because it provides insightful data on the degree of molecular contact and mixing between two separate components. The evaluated dielectric relaxation parameters from the TSDC analysis of pristine and 75 MeV oxygen ion-irradiated Kapton-H polyimide, taken under thermal windowing, are reported in this study. The TSDC of Kapton-H polyimide in the range of 20–250 °C and after exposure to 75 MeV of oxygen ion irradiation. The TSDC measurement comprises two current peaks, which occur at ~ 30 and 120 °C, respectively as shown in Fig. 9 [59]. Temperature windows have a considerable impact on the peak magnitude. The strength of the peaks in the pristine and ion-irradiated samples is impacted differently; the pristine samples exhibit an amplification in the peak, whereas the ion-irradiated samples appear to exhibit a suppression in the peak.

TSDC measurements were also used to investigate single crystals of barium titanate $BaTiO_3$ (BTO) with various orientations of (100), (110), and (111), which has proven to be a successful method for studying the fundamental connection between relaxation phenomena and defect chemistry in dielectrics [23, 60]. TSDC measurements were applied to $BaTiO_3$ single crystals that were treated under different atmospheres, and it was found that the crystal orientation and thermal treatment conditions had a remarkable effect on the defect behavior [23]. This is to investigate BTO single crystals with (100), (110), and (111) orientations, and annealed under different atmospheres, as shown in Fig. 10. The (111) crystalline face of BTO is more stable under an external field than the others.

TSDC investigated the dielectric aging of Mn and V co-doped $BaTiO_3$ multilayer ceramic capacitors (MLCC) [24]. A report by Yoon et al. claimed that Mn concentration increased with age, and V concentration had no effect based on their TSDC measurement. The low-Mn-concentration specimens with TSDC had one peak, whereas the specimens with increased Mn content displayed two peaks [24]. The first and second peaks are thought to be caused by the change in the phase of the undoped core area and the defect dipole of Mn, such as $(Mn''Ti)$-$(V_O^{\cdot\cdot})$ or $(Mn'Ti)$-$(V_O^{\cdot\cdot})$. Experiments showed that the defect dipole controls the dielectric aging rate because the Mn defect dipole has a high TSDC and a very high rate of aging.

6 Conclusions

The TSDC method is a high-resolution analysis technique that is useful for analyzing the reliability and dielectric properties of dielectric materials by analyzing the induced

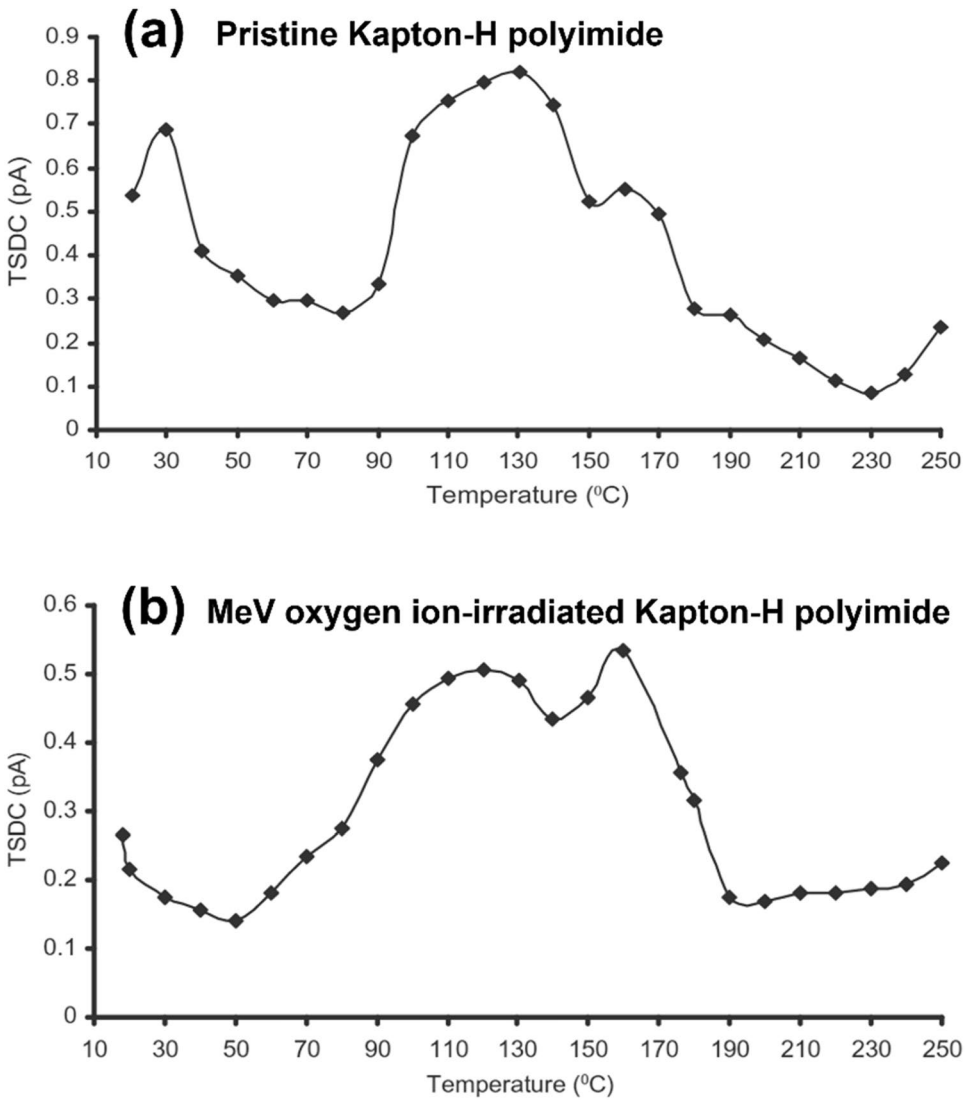

Fig. 9 Variation in TSDC for **a** pristine Kapton-H polyimide and **b** 75 MeV oxygen ion-irradiated (fluence 1.8×10^{12} ions/cm^2) Kapton-H polyimide ($E_p = 12$ kV/cm, $T_p = 90$ °C) [59]. Copyright 2011, Nuclear Instruments and Methods in Physics Research B

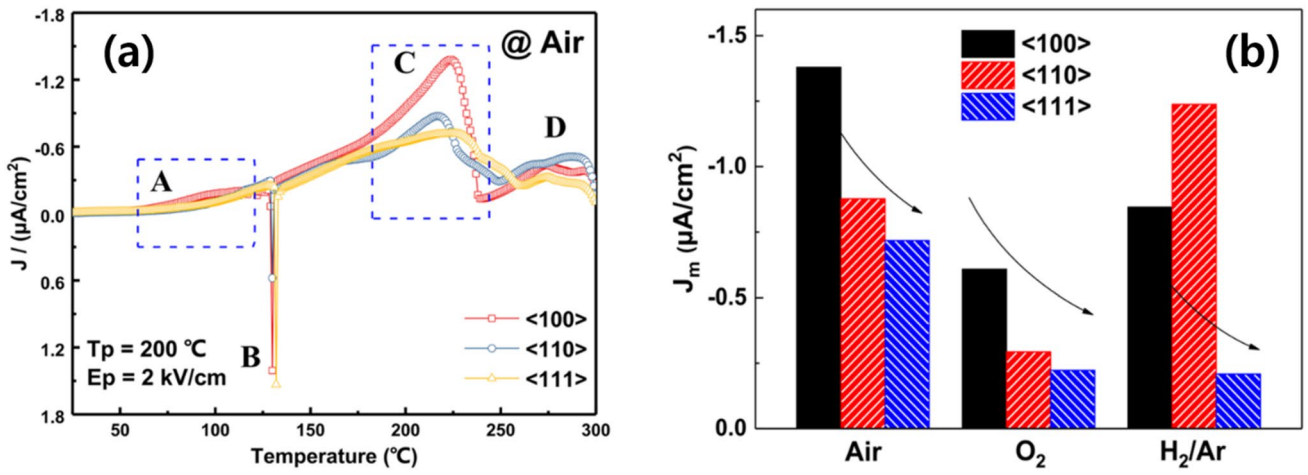

Fig. 10 **a** TSDC curves for different oriented single crystals. **b** TSDC peak density (J_m) with different oriented single crystals [23]. Copyright 2018, AIP Advances

current during relaxation, i.e., depolarization of defects by thermal stimulation. The type and concentration of defects can be confirmed by analyzing each peak of the TSDC, including information such as the peak current density (J_m) and peak temperature (T_m), and by calculating activation energy (E_a) that appears differently depending on the polarization field (E_P) and polarization temperature (T_p) during poling. Peak A in the low-temperature regime is related to the relaxation by the trap charge of the defect dipole, Peak B in the intermediate-temperature regime is related to the relaxation of the space charge by in-grain oxygen vacancies, and Peak C in the highest-temperature regime is related to the relaxation caused by the space charge of the across-grain boundary oxygen vacancies. In this review, the overall TSDC, including physical and mathematical theory, measurement method, critical factors for TSDC analysis to decide the type and concentration of defects, and various applications of TSDC, that is, polymer, ceramic, composite, and single crystal dielectrics were reviewed.

Acknowledgements This work was supported by the National Research Foundation of Korea (NRF– 2023R1A2C2005864) and Samsung Electro-Mechanics Co.

Data availability Data is available when it is rquired to the authors by contact through mail.

References

1. Y. Zhang, J. Huang, T. Ma, X. Wang, C. Deng, X. Dai, Sintering temperature dependence of energy-storage properties in (Ba, Sr) TiO3 glass-ceramics. J. Am. Ceram. Soc. **94**, 1805–1810 (2011). https://doi.org/10.1111/j.1551-2916.2010.04301.x
2. M.T. Sebastian, R. Ubic, H. Jantunen, Low-loss dielectric ceramic materials and their properties. Int. Mater. Rev. **60**, 392–412 (2015). https://doi.org/10.1179/1743280415Y.0000000007
3. X. Hao, A review on the dielectric materials for high energy-storage application. J. Adv. Dielectr. **03**, 1330001 (2013). https://doi.org/10.1142/s2010135x13300016
4. M.T. Jilani, M. Zaka, A.M. Khan, M.T. Khan, S.M. Ali, A brief review of measuring techniques for characterization of dielectric materials. Int. J. Informat.Technol. Elect. Eng. (ITEE). **1**, 1–5 (2012)
5. X. Zhang, Y. Zhang, J. Zhang, B. Peng, Z. Xie, L. Yuan, Z. Yue, L. Li, Microwave dielectric properties and thermally stimulated depolarization currents study of (1–x)Ba 0.6 Sr 0.4 La 4 Ti 4 O 15–x TiO 2 ceramics. J. Am. Ceramic Soc. **97**, 3170–3176 (2014). https://doi.org/10.1111/jace.13123
6. Y. Gao, J. Jiang, J. Wang, L. Gan, T. Zhang, Novel high-Q × f (1–x)CeO2–xCaF2 ($0.2 \leq x \leq 0.6$) microwave dielectric ceramics sintered at medium temperatures. J. Korean Ceramic Soc. **59**, 929–935 (2022). https://doi.org/10.1007/s43207-022-00223-y
7. Z. Zhao, Y. Zhang, Q. Zhang, X. Song, J. Zhu, X. Wang, Z. Zheng, Dielectric relaxation investigations in barium strontium titanate glass-ceramics: thermally stimulated depolarization current technique. Physica Status Solidi (A) Appl. Mater. Sci. **211**, 2150–2156 (2014). https://doi.org/10.1002/pssa.201431119
8. S. Priyadarshinee, J. Pati, R. Mahapatra, P. Mohanty, D.K. Mishra, J. Mohapatra, Studies of structural, microstructural, optical and dielectric properties of $GdMnO_3$. J. Korean Ceram. Soc. **60**, 203–214 (2023). https://doi.org/10.1007/s43207-022-00256-3
9. D.K. Pati, P.R. Das, B.N. Parida, B. Behera, R. Padhee, Structural, electrical, magnetic and narrow band gap-correlated optical characteristics of multiferroic [Pb(Fe0.5Nb0.5)O3]0.5–[(Ba0.8Sr0.2)TiO3]0.5. J Korean Ceramic Soc. **59**, 811–834 (2022). https://doi.org/10.1007/s43207-022-00220-1
10. X. Zang, H. Li, Y. Lu, H. Tan, H. Ji, M. Yan, Z. Liu, Dielectric properties and thermal conductivity of Si3N4–SiC composite ceramics. J. Korean Ceram. Soc. **59**, 903–908 (2022). https://doi.org/10.1007/s43207-022-00232-x
11. K.P. McKenna, A.L. Shluger, Electronic properties of defects in polycrystalline dielectric materials. Microelectron Eng. **86**, 1751–1755 (2009). https://doi.org/10.1016/j.mee.2009.03.125
12. X. Zhang, Z. Yue, B. Peng, Z. Xie, L. Yuan, J. Zhang, L. Li, Polarization response and thermally stimulated depolarization current of BaTiO 3-based Y5V ceramic multilayer capacitors. J. Am. Ceram. Soc. **97**, 2921–2927 (2014). https://doi.org/10.1111/jace.13078
13. H. Bae, Y. Shin, L. Mathur, D. Lee, S.J. Song, Defect chemistry of p-type perovskite oxide La0.2Sr0.8FeO3-δ: a combined experimental and computational study. J. Korean Ceramic Soc. **59**, 876–888 (2022). https://doi.org/10.1007/s43207-022-00237-6
14. S. Lenka, T. Badapanda, P. Nayak, S. Sarangi, S. Anwar, Compositional induced dielectric relaxation and electrical conduction behavior of samarium modified bismuth sodium titanate ceramic. Ceram Int. **47**, 5477–5486 (2021). https://doi.org/10.1016/j.ceramint.2020.10.130
15. Z. Gargar, A. Zegzouti, M. Elaatmani, A. Tachafine, D. Fasquelle, A. Outzourhit, M. Daoud, M. Afqir, Structure, electrical, and dielectric properties of $Ba1-xYxTi(1-x/4)O_3$ ceramics sintering at low temperature. J. Korean Ceram. Soc. **60**, 52–61 (2023). https://doi.org/10.1007/s43207-022-00234-9
16. A.K. Mahapatra, T. Badapanda, S. Sahoo, S. Sarangi, Investigation of structure–property correlation on the dielectric and optical properties of lanthanum modified barium titanate ceramic. J. Korean Ceram. Soc. **59**, 944–955 (2022). https://doi.org/10.1007/s43207-022-00245-6
17. W. Liu, C.A. Randall, Thermally stimulated relaxation in Fe-doped $SrTiO_3$ systems: II degradation of $SrTiO_3$ dielectrics. J. Am. Ceramic Soc. **91**, 3251–3257 (2008). https://doi.org/10.1111/j.1551-2916.2008.02613.x
18. M. Nassar, A. Elshahhat, statistical analysis of inverse Weibull constant-stress partially accelerated life tests with adaptive progressively type I censored data. Mathematics. **11**, 370 (2023). https://doi.org/10.3390/math11020370
19. S. Rahman, M. Azharuddin, J. Bansal, M. Bilal, R. Tabassum, A.K. Hafiz, Role of temperature on CdS and MoS_2 doped SnO_2 nanostructures: Potential applications in photodetection and temperature dependent current-voltage characteristics. J Alloys Compd. **941**, 168901 (2023). https://doi.org/10.1016/j.jallcom.2023.168901
20. M.U. Rehman, A. Manan, A. Ullah, Y. Iqbal, M.A. Khan, R. Muhammad, Structural, dielectric and complex impedance analysis of Pb-free BaTiO3-Bi(Mg0.5Ce0.5)O3 ceramics. J Alloys Compd. **947**, 169575 (2023). https://doi.org/10.1016/j.jallcom.2023.169575
21. B. Plotkin-Swing, G.J. Corbin, S. De Carlo, N. Dellby, C. Hoermann, M.V. Hoffman, T.C. Lovejoy, C.E. Meyer, A. Mittelberger, R. Pantelic, L. Piazza, O.L. Krivanek, Hybrid pixel direct detector for electron energy loss spectroscopy. Ultramicroscopy **217**, 113067 (2020). https://doi.org/10.1016/j.ultramic.2020.113067
22. V.D. Hodoroaba, Energy-dispersive X-ray spectroscopy (EDS), in *Characterization of Nanoparticles*. (Elsevier, 2019)

23. W. Wu, Z. Liu, Y. Gu, Z. Yue, Y. Li, Thermally stimulated depolarization current study on barium titanate single crystals. AIP Adv. **8**, 045005 (2018). https://doi.org/10.1063/1.5025501
24. S.H. Yoon, J.S. Park, S.H. Kim, D.Y. Kim, Thermally stimulated depolarization current analysis for the dielectric aging of Mn and V-codoped BaTiO3 multi-layer ceramic capacitor. Appl Phys Lett. **103**, 042901 (2013). https://doi.org/10.1063/1.4816380
25. J.J. Carter, T.J.M. Bayer, C.A. Randall, Degradation and recovery of iron doped barium titanate single crystals via modulus spectroscopy and thermally stimulated depolarization current. J. Appl. Phys. (2017). https://doi.org/10.1063/14980094
26. C.A. Randall, R. Maier, W. Qu, K. Kobayashi, K. Morita, Y. Mizuno, N. Inoue, T. Oguni, Improved reliability predictions in high permittivity dielectric oxide capacitors under high dc electric fields with oxygen vacancy induced electromigration. J Appl Phys. (2013). https://doi.org/10.1063/14772599
27. S.H. Yoon, C.A. Randall, K.H. Hur, Correlation between resistance degradation and thermally stimulated depolarization current in acceptor (Mg)-doped BaTiO3 submicrometer fine-grain ceramics. J. Am. Ceram. Soc. **93**, 1950–1956 (2010). https://doi.org/10.1111/j.1551-2916.2010.03647.x
28. S.H. Yoon, C.A. Randall, K.H. Hur, Effect of Acceptor (Mg) concentration on the resistance degradation behavior in acceptor (Mg)-doped BaTiO3 bulk ceramics: II. Thermally stimulated depolarization current analysis. J. Am. Ceram. Soc. **92**, 1766–1772 (2009). https://doi.org/10.1111/j.1551-2916.2009.03122.x
29. H. Lee, J.R. Kim, M.J. Lanagan, S. Trolier-Mckinstry, C.A. Randall, High-energy density dielectrics and capacitors for elevated temperatures: Ca (Zr, Ti) O_3. J. Am. Ceram. Soc. **96**, 1209–1213 (2013). https://doi.org/10.1111/jace.12184
30. J.C.C.A. Diaz, J.C. M'Peko, M. Venet, P.S. da Silva, Unveiling the high-temperature dielectric response of Bi 0.5Na 0.5TiO_3. Sci Rep (2020). https://doi.org/10.1038/s41598-020-75859-z
31. J. Singh, A.T. Kalghatgi, J. Parui, S.B. Krupanidhi, High-temperature dielectric response in pulsed laser deposited Bi 1.5 Zn1.0 Nb1.5 O7 thin films. J Appl Phys. Doi **10**(1063/1), 3457335 (2010)
32. J. Zhang, Z. Yue, Y. Luo, X. Zhang, L. Li, Understanding the thermally stimulated relaxation and defect behavior of Ti-containing microwave dielectrics: A case study of BaTi4O9. Mater. Des. **130**, 479–487 (2017). https://doi.org/10.1016/j.matdes.2017.05.086
33. W. Liu, C.A. Randall, Thermally stimulated relaxation in Fe-doped $SrTiO_3$ systems: I. Single crystals. J. Am. Ceram. Soc. **91**, 3245–3250 (2008). https://doi.org/10.1111/j.1551-2916.2008.02595.x
34. J.-S.P.Y.-T.K. and K.-H.H. Ji-Young Park, Thermally stimulated depolarization current test for reliability of X5R MLCC. J. Korean Ceramic Soc. **46**, 155–160 (2009). https://doi.org/10.4191/kcers.2009.46.2.155
35. W. Guo, J. Zhang, Y. Luo, Z. Yue, L. Li, Microwave dielectric properties and thermally stimulated depolarization of Al-doped Ba_4(Sm, Nd)933Ti18O54 ceramics. J. Am. Ceramic Soc. **102**, 5494–5502 (2019). https://doi.org/10.1111/jace.16448
36. Y. Luo, J. Zhang, Z. Yue, L. Li, Improvement in microwave dielectric properties of $Sr2TiO_4$ ceramics through post-annealing treatment. J Electroceram. **41**, 67–72 (2018). https://doi.org/10.1007/s10832-018-0160-z
37. X. Zhang, L. Zhang, J. Zhang, Z. Xie, L. Yuan, Z. Yue, L. Li, Dielectric response and thermally stimulated depolarization current analysis of BaNd1.76Bi0.24Ti5O14 high-temperature microwave capacitors. J. Mater. Sci. **50**, 1141–1149 (2015). https://doi.org/10.1007/s10853-014-8670-9
38. T.N.M. Ngo, U. Adem, T.T.M. Palstra, The origin of thermally stimulated depolarization currents in multiferroic $CuCrO_2$. Appl. Phys. Lett. **106**, 152904 (2015). https://doi.org/10.1063/1.4918747
39. H. Smaoui, M. Arous, H. Guermazi, S. Agnel, A. Toureille, Study of relaxations in epoxy polymer by thermally stimulated depolarization current (TSDC) and dielectric relaxation spectroscopy (DRS). J. Alloys Compd. **489**, 429–436 (2010). https://doi.org/10.1016/j.jallcom.2009.09.116
40. R.M. Neagu, E.R. Neagu, I.M. Kalogeras, A. Vassilikou-Dova, Evaluation of the dielectric parameters from TSDC spectra: application to polymeric systems. Mater. Res. Innovations **4**, 115–125 (2001). https://doi.org/10.1007/PL00010780
41. Y. Zhu, S. Li, T. Li, D. Min, B. Ma, 2015 Trap parameters analysis of oil-paper insulation by thermally stimulated depolarization current, In: Proceedings of the IEEE International Conference on Properties and Applications of Dielectric Materials, Institute of Electrical and Electronics Engineers Inc. Doi: https://doi.org/10.1109/ICPADM.2015.7295220.
42. B. Akkopru-Akgun, D.M. Marincel, K. Tsuji, T.J.M. Bayer, C.A. Randall, M.T. Lanagan, S. Trolier-McKinstry, Thermally stimulated depolarization current measurements on degraded lead zirconate titanate films. J. Am. Ceram. Soc. **104**, 5270–5280 (2021). https://doi.org/10.1111/jace.17891
43. M. Madani, N.A. Maziad, R.M. Khafagy, Thermally stimulated depolarization current and thermal analysis studies of gamma irradiated lithium-salt/polymer electrolyte blends. J. Macromol. Sci. Part B Phys. **46**, 1191–1203 (2007). https://doi.org/10.1080/00222340701629224
44. P. Photopoulos, C. Tsonos, I. Stavrakas, D. Triantis, A method for the calculation the activation energies of thermally stimulated depolarization current peaks: application in polyvinylidene fluoride/graphene nanocomposites. Physica B Condens Matter. **622**, 413338 (2021). https://doi.org/10.1016/j.physb.2021.413338
45. G. Bon Mardion, B.B. Goodman, A. Lacaze, C. Bucci, R. Fieschi, Ionic thermoconductivity method for the investigation of polarization in insulators. J. Phys. Chem. Solids. **12**, 1943 (1957). https://doi.org/10.1103/PhysRevLett.12.16
46. K.C. Shaing, K. Ida, S.A. Sabbagh, The electron trap mechanism of luminescence insulphide and silicate phosphors. Proc. Phys. Soc. **60**, 574 (1948). https://doi.org/10.1088/0959-5309/60/6/308
47. S.H. Yoon, J.B. Lim, S.H. Kim, D.Y. Kim, Influence of Dy on the dielectric aging and thermally stimulated depolarization current in Dy and Mn-codoped BaTiO3 multilayer ceramic capacitor. J. Mater. Res. **28**, 3252–3256 (2013). https://doi.org/10.1557/jmr.2013.347
48. S.H. Yoon, S.H. Kim, D.Y. Kim, Correlation between i (current)-V (voltage) characteristics and thermally stimulated depolarization current of Mn-doped BaTiO3 multilayer ceramic capacitor. J. Appl. Phys. **114**, 074102 (2013). https://doi.org/10.1063/1.4818947
49. G.M. Nasr, A.A. El-Sherif, M.M. Omar, E. Mousa, TSDC studies of LASER irradiated and unirradiated PVDF composites doped with Pd(II) benzimidazole complex. J. Multidisciplinary Eng. Sci. Technol. (JMEST). **9**, 2458–9403 (2022)
50. J.J. Moura Ramos, N.T. Correia, The determination of the activation energy of a relaxational process from thermally stimulated depolarisation currents (TSDC) data: An illustration with the β-relaxation of maltitol. Thermochim. Acta. **426**, 185–190 (2005). https://doi.org/10.1016/j.tca.2004.07.020
51. F. Namouchi, W. Jilani, H. Guermazi, Thermally stimulated depolarization current and dielectric spectroscopy used to study dipolar relaxations and trap level distribution in PMMA polymer. J. Non. Cryst. Solids. **427**, 76–82 (2015). https://doi.org/10.1016/j.jnoncrysol.2015.07.004
52. Y. Tanaka, T. Iwasaki, M. Nakamura, A. Nagai, K. Katayama, K. Yamashita, Polarization and microstructural effects of ceramic hydroxyapatite electrets. J. Appl. Phys. **107**, 014107 (2010). https://doi.org/10.1063/1.3265429

53. C.A. Nieves, A.L. Ogrinc, S.H. Kim, E. Furman, M.T. Lanagan, Ion migration study in acid-leached soda–lime–silica glass by thermally stimulated depolarization current analysis. J. Am. Ceram. Soc. (2023). https://doi.org/10.1111/jace.19064
54. Y. Shi, L. Zhang, J. Zhang, Z. Yue, Thermally stimulated depolarization currents and dielectric properties of Mg0.95Ca0.05TiO3 filled HDPE composites. AIP Adv. **7**, 125315 (2017). https://doi.org/10.1063/1.5012094
55. F. El Kamel, P. Gonon, F. Jomni, B. Yangui, Thermally stimulated currents in amorphous barium titanate thin films deposited by rf magnetron sputtering. J Appl Phys. **100**, 054107 (2006). https://doi.org/10.1063/1.2337390
56. S. Qiang, Z. Zhu, Z. Yao, H. Hao, M. Cao, H. Liu, Polarization response and thermally stimulated depolarization currents of the modified (Ba, Ca) (Zr, Ti)O3 piezoelectric ceramics. Ceram Int. (2023). https://doi.org/10.1016/j.ceramint.2023.03.027
57. D.S.B. Heidary, C.A. Randall, Li2CO3-coated Ni particles for the inner electrodes of multilayer ceramic capacitors: Evaluation of lifetime. ACS Appl. Mater. Interfaces. **9**, 585–591 (2017). https://doi.org/10.1021/acsami.6b13526
58. J. Zhang, Z. Yue, Y. Zhou, B. Peng, X. Zhang, L. Li, Temperature-dependent dielectric properties, thermally-stimulated relaxations and defect-property correlations of TiO2 ceramics for wireless passive temperature sensing. J. Eur. Ceram. Soc. **36**, 1923–1930 (2016). https://doi.org/10.1016/j.jeurceramsoc.2016.02.015
59. A. Sharma, S. Yarramaneni, J.K. Quamara, Evaluation of dielectric relaxation parameters from TSDC analysis of pristine and ion irradiated kapton-H polyimide. Nucl. Instrum. Methods Phys. Res. B. **269**, 759–763 (2011). https://doi.org/10.1016/j.nimb.2011.02.008
60. H. Qu, B. Luo, S. Bian, Z. Yue, Thermally stimulated relaxation and behaviors of oxygen vacancies in SrTiO3 single crystals with (100), (110) and (111) orientations. Mater. Res. Exp. (2020). https://doi.org/10.1088/2053-1591/ab8656